

Localization Uncertainty in Time-Intensity Stereophonic Reproduction

Enzo De Sena, *Member, IEEE*, Zoran Cvetković, *Senior Member, IEEE*, Hüseyin Hacıhabiboğlu, *Senior Member, IEEE*, Marc Moonen, *Fellow, IEEE*, Toon van Waterschoot, *Member, IEEE*

Abstract—This paper studies the effects of inter-channel time and level differences in stereophonic reproduction on perceived localization uncertainty. Towards this end, a computational model of localization uncertainty is proposed first. The model calculates inter-aural time and level difference cues, and compares them to those associated to free-field point-like sources. The comparison is carried out using a particular distance functional that replicates the increased uncertainty observed experimentally with inconsistent inter-aural time and level difference cues. The model is validated by subjective listening tests, achieving a Pearson correlation of 0.95. The model is then used to predict localization uncertainty for stereophonic setups and a listener in central and off-central positions. Results show that intensity methods achieve a slightly lower localization uncertainty for a listener positioned exactly in the center of the sweet spot. As soon as the listener moves away from that position, the situation reverses, with time-intensity methods achieving a lower localization uncertainty.

Index Terms—Stereophony, panning, recording and reproduction, localization uncertainty, auditory modelling.

I. INTRODUCTION

DESPITE significant advancements in the field of multichannel audio [3], the most common reproduction system in use today remains the two-channel stereophonic system. In typical stereophonic panning, the two loudspeakers are positioned at $\pm 30^\circ$ with respect to the listener's look direction and reproduce delayed and attenuated versions of the same signals. The differences in time and level are typically frequency-independent, and are referred to as inter-channel time difference (ICTD) and inter-channel level difference (ICLD), respectively. For ICTDs smaller than 1 ms, the listener does not perceive the two loudspeaker signals as separate, but

rather a single fused auditory event, often referred to as “phantom source”. The perceived location of the phantom source depends on both the ICTD and ICLD. This psychoacoustic effect is called “summing localization”, and is at the basis of stereophonic panning [4]. The phantom source can be moved using ICLDs alone (intensity panning), ICTDs alone (time panning) or both ICLDs and ICTDs (time-intensity panning).

Panning is inherently linked to recording. Consider a plane wave impinging on two microphones, each connected to a loudspeaker without mixing. The distance between the microphones dictates the ICTDs, while the ratio between the two directivity patterns (e.g. cardioid, figure-8) dictates the ICLDs. Recording with coincident microphones is equivalent to intensity panning, while recording with non-coincident omnidirectional microphones is equivalent to time panning. Recording with microphones that are neither omnidirectional nor coincident is equivalent to time-intensity panning.

Intensity panning is widely used in sound mixing, with most mixing desks and digital audio workstation (DAW) software implementing a version of the sine/tangent law [5], [6]. Intensity recording methods are used in a wide variety of methods, e.g. the original Blumlein pair [7], Ambisonics [8], and the spatial decomposition method [9]. While it is possible to pan a stereophonic image using time panning for certain signals, it provides higher localization uncertainty for sustained higher frequency stimuli [10].

Time-intensity recording methods such as the Decca tree [5], [7], on the other hand, are popular within the audio engineering community, mainly for their strong sense of spaciousness, which may be attributed to the higher decorrelation between the microphone signals [4], [5], [7]. While extensively used, widely-spaced microphones (in the order of meters) are often criticized for their unstable imaging [11] and irregular distribution of reproduced auditory events [7]. Near-coincident stereophonic microphones such as the ORTF and NOS pairs have also been used widely in practice [12]. These arrays are preferred by practitioners for providing a stable and natural stereophonic image. ORTF was shown to have a localization curve most similar to a binaural recording [13]. A 3D extension to ORTF was recently proposed [14] and was shown to provide a good overall localization and auditory spaciousness in comparison with a coincident recording setup [15].

More recent work on time-intensity recording techniques generally consider the problem from a constrained perspective, by using standard microphone directivities, by evaluating

Enzo De Sena is with the Institute of Sound Recording at the University of Surrey (UK) (e.desena@surrey.ac.uk). Zoran Cvetković is with the Department of Informatics at King's College London (UK). Hüseyin Hacıhabiboğlu is with the Graduate School of Informatics, Middle East Technical University (METU), Ankara, TR-06800, Turkey. Marc Moonen and Toon van Waterschoot are with the Department of Electrical Engineering at KU Leuven (Belgium). The work reported in this paper was partially funded by (i) EPSRC Grant EP/F001142/1, (ii) European Commission under Grant Agreement no. 316969 within the FP7-PEOPLE Marie Curie Initial Training Network “Dereverberation and Reverberation of Audio, Music, and Speech (DREAMS)” (iii) European Research Council under the European Union's Horizon 2020 research and innovation program/ERC Consolidator Grant: SONORA (no. 773268), (iv) KU Leuven internal funds C2-16-00449 “Distributed Digital Signal Processing for Ad-hoc Wireless Local Area Audio Networking”. This paper reflects only the authors' views and the Union is not liable for any use that may be made of the contained information. The authors would like to thank Niccolò Antonello for pointing out that the proposed computational model has a statistical interpretation. Parts of this work were previously presented in [1] and [2].

spatial acuity only at the sweet spot, or both. For example, a psychoacoustical evaluation of equal segment microphone array (ESMA) [16], revealed that the selection of the recording array dimensions has a distinct effect on the localization accuracy for an ESMA using cardioid microphones [17]. In another subjective study, first-order Ambisonics with *max-rE* encoding provided lower stereophonic image shifts in comparison with ESMA for a central listening position [18].

While the design of microphone arrays for recording spatial audio has traditionally been an *ad hoc* process driven by practical evidence that is not necessarily objectively validated, systematic approaches have also been proposed. A recently proposed design tool called microphone array recording and reproduction simulator (MARRS) allows the designer to design a stereophonic microphone pair using standard microphone directivity patterns (e.g. cardioid) and to observe the performance of the design both by visualization of the resulting localization curves and auralization of the simulation [19].

A similar systematic framework for the design of intensity and time-intensity circular multichannel recording and reproduction systems was proposed in [20], based on earlier work [21], [22]. An objective analysis based on active intensity fields showed that for stable rendition of plane waves it is beneficial to render each such wave by no more than two loudspeakers, thus re-framing the multichannel problem as a stereophonic one. Using available psychoacoustic curves, a family of optimal microphone directivity patterns was obtained, parametrized by the array radius. The obtained directivity patterns are too spatially selective to be implemented using first-order microphone patterns (e.g. hypercardioid), but can be implemented using higher-order microphones, e.g. differential microphones [23], [24]. Formal listening experiments were carried out for a microphone array with 15.5 cm radius [20]. Results showed a significantly improved localization accuracy with respect to Johnston's array, and comparable to that of vector-base amplitude panning (VBAP) and Ambisonics when the listener is in the center of the loudspeaker array. The experiments also assessed the localization uncertainty, defined as how difficult it is for the listener to tell where the sound source is located. Results showed an improvement in localization uncertainty with respect to VBAP and Ambisonics when the listener is in a position 30 cm off-center.

This paper explains why that is the case and shows that this is a more general characteristic of time-intensity methods. Towards this end, this paper proposes a computational model of localization uncertainty (the model also allows prediction of the perceived direction, but this is left for future work).

Formal listening experiments require very careful design and carrying them out is expensive and time-consuming [25]. Computational models provide a fast and repeatable alternative. Spatial hearing involves several stages of processing of sound waves impinging on the listener's head, which have been the subject of intensive study over the years. Well-established models now exist for the early stages of the mechanisms of spatial hearing, such as the effects of head diffraction, cochlear filtering and neural transduction. On the other hand, the higher levels of processing, where the spatial cues are combined, are not well understood yet. Various models have been proposed in

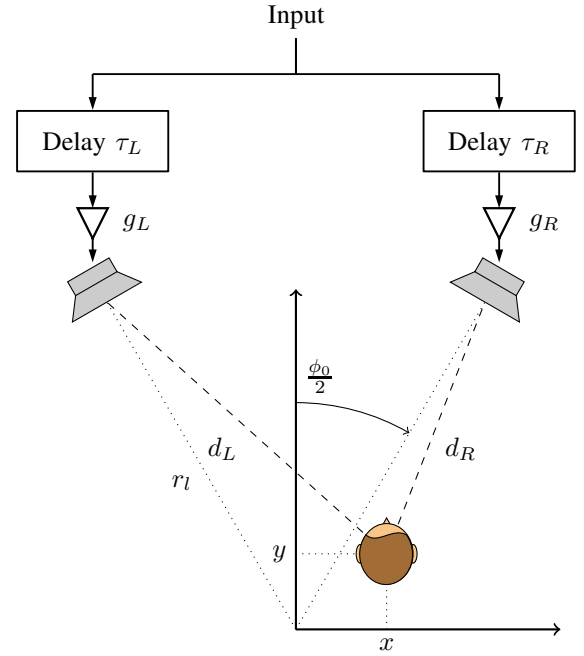


Fig. 1: Stereophonic reproduction system.

the literature, but none has proved to be capable of predicting all characteristics of human hearing. This paper proposes a model that first calculates interaural time difference (ITD) and interaural level difference (ILD) cues and then compares them to the ones associated to point-like sources. The comparison is carried out using a distance function which replicates the auditory event splitting observed with inconsistent ITD-ILD cues. It is shown that predictions of localization uncertainty based on this model are highly correlated with subjective scores. This model is then applied to generic ICTD-ICLD values in central and off-central positions to assess how time-intensity stereophony affects localization uncertainty.

The paper is organized as follows. Section II provides the background on time-intensity stereophony and on auditory system modelling. Section III presents the proposed model to predict localization uncertainty. Section IV discusses how time-intensity panning affects localization uncertainty in stereophonic reproduction. Section V narrows the focus on a specific family of time-intensity panning curves proposed in [20]. Section VI concludes the paper.

II. BACKGROUND

A. Stereophonic Reproduction

Consider a stereophonic reproduction setup as shown in Fig. 1 with base angle ϕ_0 and loudspeaker distance r_l . The two loudspeakers are reproducing delayed and attenuated versions of the same signal. The gains applied to the left and right loudspeaker are denoted as g_L and g_R , respectively, while the delays are τ_L and τ_R . The ICLD is defined as $ICLD = 20 \log_{10} \frac{g_L}{g_R} = G_L - G_R$, where $G_L = 20 \log_{10} g_L$ and $G_R = 20 \log_{10} g_R$. The ICTD, on the other hand, is defined as $\tau_R - \tau_L$. Notice how these definitions are given such that whenever

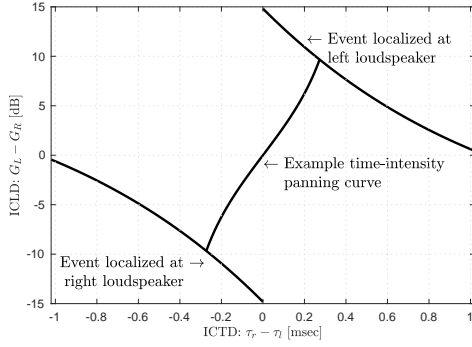


Fig. 2: Williams' psychoacoustic curves, together with the panning curve associated to the perceptual sound-field reconstruction (PSR) method with 0.187 m array radius. Intensity methods are associated to points on the y-axis (ICTD = 0 ms).

ICTD and ICLD have the same sign, their effect is consistent to one another. For instance, when both are positive, the left loudspeaker is louder and its signal also arrives earlier.

If the ICTD is below the *echo threshold*, the listener will perceive a single fused auditory event [4]. The echo threshold is strongly stimulus-dependent, and varies between 2 ms (for clicks) and 40 ms (for speech) [4]. For ICTDs between 1 ms and the echo threshold, the auditory event is localised at the loudspeaker whose signal arrives first [4], [26]. This effect is called “law of the first front” [27]. For ICTDs smaller than 1 ms, a single fused “phantom” sound source is localised in a position that depends on both ICTD and ICLD. This psychoacoustic effect is called “summing localization” [4]. In the literature, summing localization and the law of the first front are collectively referred to as “precedence effect” [4].

Fig. 2 shows Williams's time-intensity psychoacoustic curves, which represent all the ICLD-ICTD pairs that render the phantom source in the direction of the left and right loudspeaker [28]. Other time-intensity psychoacoustic curves are also available in the literature [5], [29], [30].

The psychoacoustic curves show that if one wishes to render a phantom source in the direction of the left (respectively, right) loudspeaker it is possible to use an ICLD of about 15 dB (respectively, -15 dB) without any ICTD (intensity panning). It is then possible to continuously pan between the two loudspeakers using ICLDs that vary between these two extremes (notice that the psychoacoustic curves do not give information on how to do this exactly, and only provide information about the extreme directions). Fig. 2 also shows that it is possible to render a sound source in the direction of the left loudspeaker by reducing the ICLD but increasing the ICTD (time-intensity panning). If the ICLD is reduced to zero (time panning), it is still possible to displace the phantom source all the way to the left (respectively, right) loudspeaker with an ICTD of about 1 ms (respectively, -1 ms), which corresponds to the onset of the law of the first front.

B. Stereophonic recording

The first systematic approach to the problem of two-channel stereophonic recording is attributed to Blumlein [5], [7]. The Blumlein pair consists of two coincident figure-8 microphones

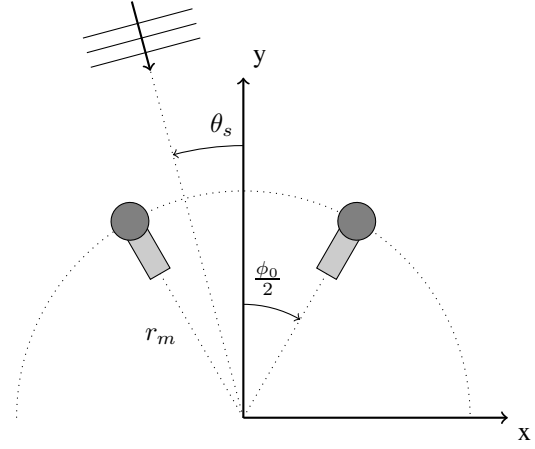


Fig. 3: Stereophonic recording system.

positioned orthogonally to each other. Here, each microphone is connected to the corresponding loudspeaker, without mixing. Systems without mixing are also the focus of the rest of this paper. Here, inter-microphone time and level differences are thus identical to ICTDs and ICLDs, respectively. In the specific case of the Blumlein pair, the ICTDs are zero, since the microphone pair is coincident.

A variety of stereophonic arrangements have been proposed in the past few decades (see e.g. [5], [7]), mostly designed on a trial-and-error basis. A systematic framework for the design of circular microphone arrays was proposed in [20], which is summarized in the next section.

C. Perceptual Soundfield Reconstruction

This section summarizes the procedure proposed in [20], but for the specific case of the stereophonic setup. The objective here is to define a panning curve, which is characterized by the two functions $\text{ICTD}(\theta_s)$ and $\text{ICLD}(\theta_s)$, where θ_s is the intended direction of the auditory event.

Consider Fig. 3. Here, the microphones are positioned on a circle with radius r_m facing outwards. The angle separating the two microphones is ϕ_0 , and θ_s is the angle of an incoming plane wave. Each microphone is connected to a corresponding loudspeaker. The inter-microphone delay (and thus ICTD) is:

$$\text{ICTD}(\theta_s) = 2 \frac{r_m}{c} \sin\left(\frac{\phi_0}{2}\right) \sin\theta_s, \quad (1)$$

where c is the speed of sound ($c = 343$ m/s in dry air at 20°). Consider the ICTD obtained for a plane wave with $\theta_s = \frac{\phi_0}{2}$, i.e. in the direction of the left microphone:

$$\text{ICTD}(\phi_0/2) = 2 \frac{r_m}{c} \sin^2\left(\frac{\phi_0}{2}\right). \quad (2)$$

Given the value of $\text{ICTD}(\phi_0/2)$, psychoacoustic time-intensity curves can be used to find the minimum ICLD necessary to render a phantom source in the direction of the left loudspeaker. Rather than using Franssen curves as in [20], which are considered to be not sufficiently precise for quantitative design [4], this paper uses Williams curves. The curve associated to the event being localized at the left loudspeaker

can be well approximated by the following sigmoid function (obtained using Matlab's curve fitting toolbox):

$$\text{ICLD}_{W,L}(\text{ICTD}) = 221.59 - \frac{230.18}{1 + e^{-1000\text{ICTD} + 2.1786}} \cdot (3)$$

Setting the ICLD to be equal to the Williams value yields the constraint $\text{ICLD}(\phi_0/2) = \text{ICLD}_{W,L}(\text{ICTD}(\phi_0/2))$. The value $\text{ICLD}_{W,L}(\text{ICTD}(\phi_0/2))$ will be denoted by ICLD_W in the following. For $\theta_s = -\frac{\phi_0}{2}$ (i.e. the direction of the right loudspeaker) one has $\text{ICLD}(-\phi_0/2) = \text{ICLD}_{W,R}(\text{ICTD}(-\phi_0/2))$, which, due to the symmetry of the problem, is equivalent to $\text{ICLD}(-\phi_0/2) = -\text{ICLD}_W$. A third trivial point can be added, i.e. $\text{ICLD}(0) = 0$ dB.

It remains to choose how to connect these three points. Two choices were explored in [20]: a simple straight line [31], or a modified version of the tangent panning law [20]. While both approaches were shown to lead to a good localization accuracy (i.e. the phantom source was shown to be perceived close to the intended direction θ_s), the latter approach allows to link the design with other methods (e.g. VBAP [6]) and consists of the following parametric function:

$$\text{ICLD}(\theta_s) = 20 \log_{10} \frac{\sin\left(\frac{\phi_0}{2} + \beta + \theta_s\right)}{\sin\left(\frac{\phi_0}{2} + \beta - \theta_s\right)}, \quad (4)$$

where β is a free parameter that is used to satisfy the constraint $\text{ICLD}(\phi_0/2) = \text{ICLD}_W$ (the other two points are then also satisfied due to symmetry), which results in

$$\beta = \arctan\left(\frac{10^{\frac{\text{ICLD}_W}{20}} \sin(\phi_0)}{1 - 10^{\frac{\text{ICLD}_W}{20}} \cos(\phi_0)}\right). \quad (5)$$

To summarize, to obtain the PSR panning curve one should (a) set the free parameter r_m , (b) obtain $\text{ICTD}(\phi_0/2)$ from (2), (c) obtain ICLD_W from (3) and β from (5) and (d) obtain $\text{ICTD}(\theta_s)$ and $\text{ICLD}(\theta_s)$ from (1) and (4), respectively. Fig. 2 shows the panning curve obtained for $r_m = 0.187$ m.

The so-obtained $\text{ICLD}(\theta_s)$ and $\text{ICTD}(\theta_s)$ can be viewed either in the context of stereophonic panning, whereby they can be used to directly control appropriate loudspeaker gains and delays, or in the context of stereophonic recording. In the latter case, the microphone directivity patterns can be designed so as to emulate $\text{ICLD}(\theta_s)$. Thus, one wishes to set $\text{ICLD}(\theta_s) = 20 \log_{10} \frac{\Gamma_L(\theta_s)}{\Gamma_R(\theta_s)}$, where $\Gamma_L(\theta_s)$ and $\Gamma_R(\theta_s)$ denote the directivity patterns of the left and right microphones. In general, first-order microphones (i.e. microphones with $\Gamma(\theta_s)$ of the type $\Gamma(\theta_s) = a_0 + a_1 \cos(\theta_s)$) are not sufficiently directive to achieve the necessary ICLDs. Second-order microphones are already sufficient for this purpose [20].

D. Auditory system modelling

The auditory system estimates the directions of sound sources based on a combination of monaural and binaural cues [4]. Localization in the horizontal plane is mostly reliant on binaural cues, particularly on differences in the time of arrival and on difference in level of a sound wave at the two ears. ITDs are caused by the different time of arrival of sound waves radiated by sources outside the median plane. At

low frequencies the auditory system analyses the interaural time difference between the signals' fine structure [4]. At higher frequencies this mechanism becomes ambiguous, and the time differences between the signals' envelopes are used instead [4]. The maximum naturally occurring ITD is approximately 0.65 ms [4], [5]. ILDs are caused by the acoustical shadowing of the head and are strongly frequency-dependent. At low frequencies the head is approximately transparent to the sound wave and the level differences are small. As the wavelength approaches the size of the human head, the level differences become sensible. The highest natural ILD is in the region of 20 dB [4].

A common confusion in this context is to assume that ICTDs are identical to ITDs, and ICLDs are identical to ILDs, which is incorrect. The wavefronts of each loudspeaker reach both ears and form interference patterns at the position of the ears, which, in turn, lead to a complex relationship between ICTD-ICLD and ITD-ILD. Also notice that, as opposed to ICTDs and ICLDs, ITDs and ILDs are frequency-dependent.

The mechanisms by which the auditory system interprets the ITD and ILD cues are complex and not yet fully understood [4]. Experimental evidence suggests that humans use two main mechanisms for source localization, and that these mechanisms are to a certain degree independent from one another [4, p.173]. The first interprets the interaural time shifts between the signals' fine structure and uses signal components below 1.6 kHz. The second interprets the interaural level differences and time shifts of the envelopes *jointly*. The latter mechanism seems to be dominant for signals with significant frequency content above 1.6 kHz [4, p.173].

A first, most notable attempt to model binaural processing was made by Jeffress in 1948 [32], who hypothesised that sound localization is governed by a mechanism of running cross-correlation between the two channels. While today this is still considered to be an adequate mean of measuring ITDs, it does not account for the presence of ILDs [4]. Lindemann [33] proposed a model that incorporates this information in the cross-correlation mechanism by way of inhibitory elements that are physiologically plausible. Gaik [34] extended this model further, based on the observation that ITDs and ILDs due to point-like sources in free field come in specific pairs. For instance the ITD and ILD values for a source in the median plane are both small. On the other hand, for a source to the right/left, both ITD and ILD are high. In fact, in these cases the acoustic wave arriving at the far ear is both attenuated (because of head shadowing) and delayed (because of propagation time).

Gaik observed that when inconsistent ITD-ILD pairs (e.g. a left-leading ILD and a right-leading ITD) are presented over headphones, the auditory event width increases, and sometimes two separate events appear [4], [34]. In other words, inconsistent ITD-ILD pairs cause increased localization uncertainty. These unnatural conditions can arise also with multiple sources radiating coherent signals, as in stereophonic reproduction. Indeed, although each loudspeaker acts as a free-field source, the signals due to the different loudspeakers add up at the ears, creating interference phenomena that may result in inconsistent ITD-ILD cues. Quantifying the deviation between the

reproduced ITD-ILD pairs and the ones associated to natural sources is therefore useful to study the localization uncertainty due to different multichannel methods. A study presented by Pulkki and Hirvonen in [35] goes in this direction. For a given multichannel method they find the angle of the closest free-field source in terms of ILD and ITD, separately. This model gives useful predictions when the angles corresponding to the ILD and to the ITD coincide. However, in most cases the ITD and ILD cues provide contradicting information, and therefore the model output is hard to interpret [35].

III. LOCALIZATION UNCERTAINTY MODEL

The first step of the model is to calculate ITD-ILD pairs of single point-like free-field sound sources in a number of directions on the horizontal plane. The so-obtained pairs are referred to as *free-field ITD-ILD pairs*. Similarly to [35] and [36], it is hypothesized here that the auditory system uses the free-field ITD-ILD pairs as a dictionary to interpret all other acoustical conditions. The ITD-ILD pairs for the acoustical scene to be estimated are calculated and compared to the free-field ITD-ILD pairs using a given distance functional. Finally, the information is combined across critical bands to obtain an overall estimate of the localization uncertainty.

A. Calculation of ILDs and ITDs

In this paper, the source-to-ear transfer functions are obtained using the spherical head model proposed in [37]. The source stimulus is a 50 ms long pink noise sample, multiplied by a Tukey window with taper parameter 5% (which is also used in the other simulations in this paper). The sampling frequency is 44.1 kHz. Each simulation is repeated five times to average out the effect of different pink noise realizations.

As mentioned earlier in Section II-D, the mechanism that interprets the interaural level differences and time shifts of the envelopes *jointly* is dominant for signals with significant frequency content above 1.6 kHz. Furthermore, while ITDs are evaluated across the audible spectrum, ILDs have greater importance for signals with significant frequency content above 1.6 kHz [4, p.166]. It is then hypothesized here that the greatest contribution to localization uncertainty is due to inconsistencies between the interaural cues above 1.6 kHz, which is a frequency region where both cues are significant.

The response of the cochlea is modelled using a gammatone filter-bank [38] with 24 center frequencies equally spaced on the equivalent rectangular bandwidth (ERB) scale between 1.6 kHz and 15 kHz [39]. As a rough model of the neuron firing probability smoothing at high frequency, the envelope of each bandpass signal is taken using the discrete Hilbert transform [34]. The resulting signals are fed to 24 binaural processors that calculate the ITD and ILD values independently. The ITD is calculated as the location of the maximum of the cross-correlation function evaluated over time lags between $[-0.7, 0.7]$ ms [34], [36]. The ILD is calculated as the energy ratio of the left and right channel [36]. Altogether, the model produces a set of 24 ITD-ILD pairs (48 values in total).

Fig. 4 show the ITD-ILD pairs associated to free-field sources in the frontal horizontal plane. Each point corresponds

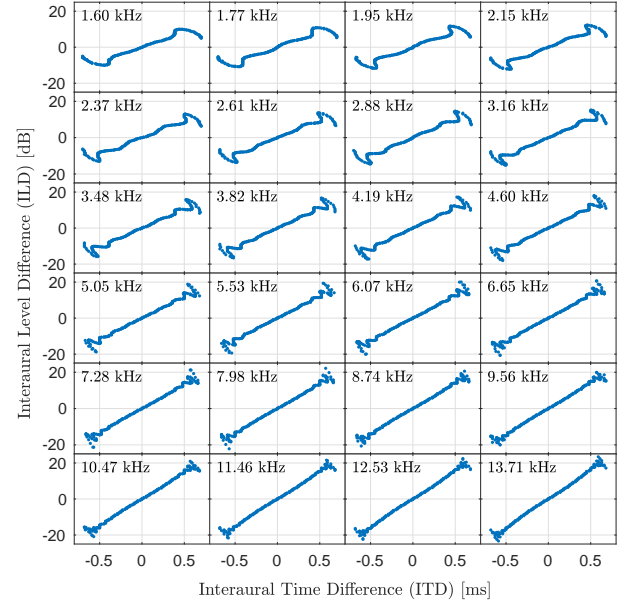


Fig. 4: The figure shows the ITD-ILD pairs associated to point-like free-field sources in each critical band.

to a free field source positioned 2 m away from the listener and with angles between $\theta = -90^\circ$ and $\theta = 90^\circ$ with an angular resolution of 1° . In the remainder of this paper, these values will be denoted as $\text{FITD}_i(\theta)$ and $\text{FILD}_i(\theta)$, respectively, where i is the critical band index and θ is the free-field source angle with respect to the listener's look direction.

It can be observed in Fig. 4 that the interaural cues are highly correlated, i.e. larger ITD values are typically associated to larger ILD values, which is due to the concurrent effect of sound propagation and diffraction around the head [34]. Also, the maximum ILD values increase with frequency, which is due to the increasing head shadowing associated to decreasing wave lengths [34].

B. Distance between ITD-ILD pairs

Let ILD_i and ITD_i denote the ITD and ILD values in the i -th critical band as observed by a listener under stereophonic reproduction (or other acoustical conditions).

In order to combine the information of ITD and ILD cues across critical bands, it is useful to normalize all quantities to the maximum values of the free-field cues:

$$\overline{\text{ITD}}_i = \frac{\text{ITD}_i}{\max_{\theta} |\text{FITD}_i(\theta)|} \quad (6)$$

$$\overline{\text{ILD}}_i = \frac{\text{ILD}_i}{\max_{\theta} |\text{FILD}_i(\theta)|} \quad (7)$$

The free-field pairs $\text{FITD}_i(\theta)$ and $\text{FILD}_i(\theta)$ are normalized in the same way and are denoted as $\overline{\text{FITD}}_i(\theta)$ and $\overline{\text{FILD}}_i(\theta)$, respectively.

Notice that while $\overline{\text{FITD}}_i(\theta) \in [-1, 1]$ and $\overline{\text{FILD}}_i(\theta) \in [-1, 1]$, $\overline{\text{ITD}}_i$ and $\overline{\text{ILD}}_i$ can in theory be outside that range. Indeed, there is no guarantee that the acoustical condition being analyzed has ITD-ILD values outside the range of values occurring for free-field sources.

The aim is now to select a distance functional between

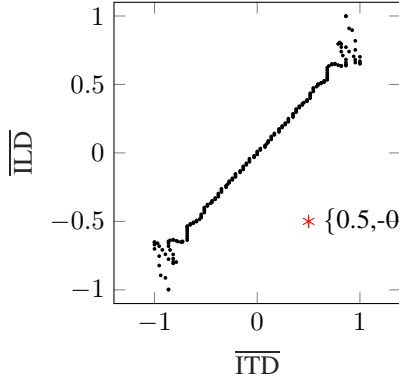


Fig. 5: The figure shows the normalized ITD and ILD pairs associated to free-field sources for the 15th critical band (black dots), and an example of a $\{\overline{\text{ITD}}, \overline{\text{ILD}}\}$ point in $\{0.5, -0.5\}$.

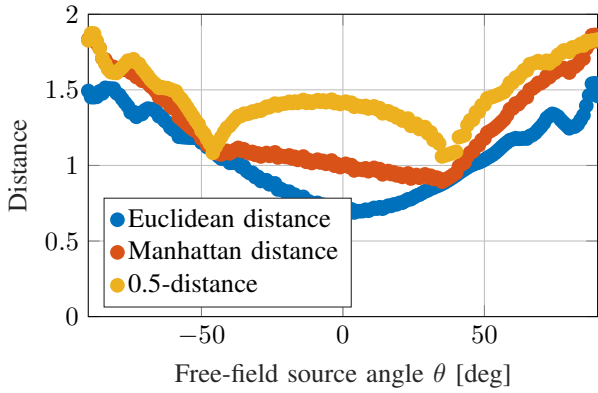


Fig. 6: Distance between $\{\overline{\text{ITD}}_{15}, \overline{\text{ILD}}_{15}\} = \{0.5, -0.5\}$ and the free-field point $\{\overline{\text{FITD}}_{15}(\theta), \overline{\text{FILD}}_{15}(\theta)\}$ as a function of direction θ and for different distance functionals.

$\{\overline{\text{ITD}}_i, \overline{\text{ILD}}_i\}$ and $\{\overline{\text{FITD}}_i(\theta), \overline{\text{FILD}}_i(\theta)\}$ according to some meaningful psychoacoustic criterion. Consider the distance defined by the classical p -norm:

$$\xi_i(\theta) = \left[|\overline{\text{ITD}}_i - \overline{\text{FITD}}_i(\theta)|^p + |\overline{\text{ILD}}_i - \overline{\text{FILD}}_i(\theta)|^p \right]^{\frac{1}{p}}. \quad (8)$$

Fig. 5 shows an example of an observed $\{\overline{\text{ITD}}_{15}, \overline{\text{ILD}}_{15}\}$ point positioned at $\{0.5, -0.5\}$ in the 15th critical band (the one centered at 6.07 kHz). The distance between each free-field source $\{\overline{\text{FITD}}_{15}(\theta), \overline{\text{FILD}}_{15}(\theta)\}$ and the $\{\overline{\text{ITD}}_{15}, \overline{\text{ILD}}_{15}\} = \{0.5, -0.5\}$ point is plotted in Fig. 6 as a function of the free-field source angle, θ , for different distance functionals.

The experimental evidence shows that subjects presented with contradicting ITD-ILD pairs are likely to report split auditory events [34]. The Euclidean distance ($p = 2$) does not emulate this behaviour, as it leads to a single minimum in $\theta = 0$, as shown in Fig. 6. The Manhattan distance ($p = 1$) is nearly constant in the $[-30^\circ, 30^\circ]$ angular sector. The 0.5-distance, on the other hand, causes two sharp minima, one of which is centred in the direction corresponding to the ITD cue, which is compatible with the psychoacoustic evidence [4, p.170]. Other values of p close to 0.5 would also retain this behaviour. In the next section it is shown that the model has

very good predictive power even without careful tuning of p .

The functional defined in (8) does not satisfy the triangle inequality for $p < 1$. However, the same distance raised to power p , i.e. $\xi_i^p(\theta)$, does satisfy all the properties of a distance [40]. Hence, the p -norm distance used here is:

$$d_i(\theta | \overline{\text{ITD}}_i, \overline{\text{ILD}}_i) = |\overline{\text{ITD}}_i - \overline{\text{FITD}}_i(\theta)|^p + |\overline{\text{ILD}}_i - \overline{\text{FILD}}_i(\theta)|^p. \quad (9)$$

The objective is to obtain a function of θ that quantifies the likelihood that a sound is perceived in that direction. Intuitively, this function should be inversely proportional to $d_i(\theta | \overline{\text{ITD}}_i, \overline{\text{ILD}}_i)$, such that whenever the distance is small, the likelihood is high (and viceversa). Let this function be

$$f_i(\theta | \overline{\text{ITD}}_i, \overline{\text{ILD}}_i) = K e^{-d_i(\theta | \overline{\text{ITD}}_i, \overline{\text{ILD}}_i)}, \quad (10)$$

where K is a positive constant. Although other choices are available (e.g. [1] uses $\max_\theta(d_i(\theta)) - d_i(\theta)$), the advantage of (10) is that it gives the model an explicit statistical interpretation in the maximum likelihood (ML) framework, as will be discussed in the next subsection.

The next step is to integrate the information from the different critical bands. Since the mechanisms governing this stage of perception are generally regarded as complex and not well understood [4], [35], the information across critical bands is combined conservatively using the simple average:

$$f(\theta | \overline{\text{ITD}}, \overline{\text{ILD}}) = \frac{K}{N} \sum_{i=1}^N e^{-d_i(\theta | \overline{\text{ITD}}_i, \overline{\text{ILD}}_i)}, \quad (11)$$

where $\overline{\text{ILD}}$ denotes the vector $\overline{\text{ILD}} = [\overline{\text{ILD}}_1, \dots, \overline{\text{ILD}}_N]$ and $\overline{\text{ITD}} = [\overline{\text{ITD}}_1, \dots, \overline{\text{ITD}}_N]$, and N is the number of critical bands ($N = 24$).

C. Statistical interpretation

Suppose that $\{\overline{\text{ITD}}_i, \overline{\text{ILD}}_i\}$ are noisy observations of a point-like free-field source at angle θ_0 associated to a set of true $\{\overline{\text{FILD}}_i(\theta_0), \overline{\text{FITD}}_i(\theta_0)\}$ values:

$$\begin{aligned} \overline{\text{ITD}}_i &= \overline{\text{FITD}}_i(\theta_0) + u_i, \\ \overline{\text{ILD}}_i &= \overline{\text{FILD}}_i(\theta_0) + v_i. \end{aligned} \quad (12)$$

where u_i and v_i are the noise components, which may arise for instance as a consequence of room reverberation or reproduction with multiple loudspeakers. Let the joint distribution of the noise components be the following mixture of zero-mean bivariate theta-generalized normal distributions [41]:

$$f(u_1, \dots, u_N; v_1, \dots, v_N) = \frac{1}{N} \sum_{i=1}^N C e^{-\frac{|u_i|^p + |v_i|^p}{2\sigma^2}}, \quad (13)$$

where σ represents a standard deviation and $C = [2\Gamma(1 + 1/p)^n (2\sigma^2)^{2/p}]^{-1}$.

Notice that if $\frac{1}{2\sigma^2} = 1$, equation (13) becomes formally identical to (11). Suppose now that the auditory system estimates the true value θ_0 using an ML approach. Within this context, $f(\theta | \overline{\text{ITD}}, \overline{\text{ILD}})$, seen here as a function of θ , formally takes the meaning of a likelihood function.

Although the objective of the proposed model is not to estimate θ itself (which is left for future work), the shape of the likelihood function gives information about how difficult it is to estimate it, as will be explained in the next subsection.

D. Calculation of the localization uncertainty

The likelihood function quantifies the probability that a subject would perceive a source in a given direction θ . From this perspective, a uniform (constant) likelihood function would result in a maximally uncertain (diffuse) event. At the other extreme, an impulsive likelihood function would result in a minimally uncertain event. Various measures can be used to measure this quantity. One of them is Wiener entropy (also known as spectral flatness), which is defined as the ratio of the geometric mean over the arithmetic mean [42]:

$$H(\overline{\text{ITD}}, \overline{\text{ILD}}) = \frac{\sqrt[K]{\prod_{k=1}^K f(\theta_k | \overline{\text{ITD}}, \overline{\text{ILD}})}}{\frac{1}{K} \sum_{k=1}^K f(\theta_k | \overline{\text{ITD}}, \overline{\text{ILD}})}, \quad (14)$$

where θ_k are the angles of the considered free-field sources, and K is their cardinality. This measure takes values between 0, which is associated to an impulsive function, and 1, which is associated to a constant function.

The final step is to normalize the value of H . Indeed, since $f(\theta_k | \overline{\text{ITD}}, \overline{\text{ILD}})$ is never impulsive (even for free-field sources), the value of H is always larger than zero. For instance, for $p = 0.3$, the minimum H is 0.85. The following normalization yields values close to zero for estimates associated to free-field sources:

$$\overline{H}(\overline{\text{ITD}}, \overline{\text{ILD}}) = \frac{H(\overline{\text{ITD}}, \overline{\text{ILD}}) - H_{\min}}{1 - H_{\min}} \quad (15)$$

where $\overline{H}(\overline{\text{ITD}}, \overline{\text{ILD}})$ denotes the estimates of the proposed model and $H_{\min} = \min_k H(\overline{\text{ITD}}(\theta_k), \overline{\text{ILD}}(\theta_k))$.

It is noted that two alternative approaches have also been considered but have not been further pursued. The first approach involves normalizing the likelihood function such that it sums up to one, and then using the information-theoretical definition of entropy of a probability mass function. This approach yields a similar performance to (14). The second approach stems from the result that the ML estimator of θ is asymptotically distributed as $\hat{\theta} \sim \mathcal{N}(\theta, I^{-1}(\theta))$, where $I(\theta)$ is the Fisher information evaluated in θ [43, p. 167]. The 95% confidence interval of the ML estimator is therefore $\hat{\theta} \pm \frac{1.96}{\sqrt{Q I(\theta)}}$, where Q is the number of observations. This measure does not perform well as an estimate of localization uncertainty, which is likely due to the fact that the model has access to a single observation (i.e. $Q = 1$) and thus the asymptotic assumption is not valid.

E. Model validation

A subjective listening test with 19 subjects was carried out in [20] using a modified MUSHRA test [44]. The subjects answered the question “How certain are you of the direction of the source?” by giving a score on a continuous scale from 0 to 100. The test was carried out in an audio booth using four synthesized 5-channel surround sound methods: (a) pair-wise tangent panning law [45] (equivalent to horizontal VBAP); (b) near-field corrected second-order Ambisonics with mode-matching decoding at low frequency and maximum-energy decoding at high frequency [8], [46], [47]; (c) second-order Ambisonics with in-phase decoding [48]; and (d) the

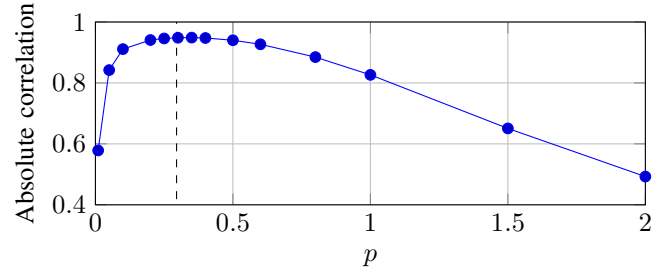


Fig. 7: Absolute Pearson correlation between the model predictions and the testing set as a function of the distance functional parameter p . The dashed vertical line denotes the value chosen in the remainder of the simulations in this paper.

quasi-coincident microphone array proposed in [20]. The test was run for three sound source directions and two seating positions, and included both a reference (a loudspeaker in the intended direction) and an anchor (an approximately diffused soundfield). Details of the experiment are available in [20].

In order to validate the proposed model, the experiment was replicated here through simulations. First, for each loudspeaker, the ear pressure signals were obtained using the spherical head model proposed in [37] in simulated free-field conditions. Appropriate time delays were added in case the simulated head was in the off-center position. Second, the ear pressure signals associated to the two loudspeakers were added together.

The resulting ear pressure signals were then fed to the proposed model and localization uncertainty estimates were obtained using (15). Fig. 7 shows the absolute Pearson correlation between the subjective scores and the localization uncertainty estimates, as a function of the parameter p . The Pearson correlation is approximately -0.95 for $p \in [0.25, 0.35]$, confirming that the model predictions are strongly correlated with the experimental data. The reason why the correlation is negative is that subjects’ answers to the question “How certain are you of the direction of the source?” are merely inverted with respect to localization uncertainty.

Similar results are obtained (a) if the spherical head model is replaced with measured head related transfer functions (HRTFs) [49], (b) if instead of the exponential function in (10) one uses $\max_{\theta} (d_i(\theta)) - d_i(\theta)$ as in [1] and (c) if instead of the Wiener entropy in (14), one uses the information-theoretical entropy after normalization.

Fine tuning of the p -norm distance is also not critical as long as contradicting ITD-ILD cues lead to a bimodal likelihood function. Values of p between 0.2 and 0.5 all give correlation coefficients stronger than -0.94 . A correlation of -0.83 is obtained with the Manhattan distance ($p = 1$). The Euclidean distance ($p = 2$), on the other hand, yields a much weaker correlation of -0.49 . At the other extreme, a small p also leads to weak correlations, indicating that norms closer to the l_0 -norm do not provide an effective measure in this context.

The value chosen for the simulations in the remainder of this paper is $p = 0.3$, i.e. the mid-point of the $p \in [0.25, 0.35]$ range with ≈ -0.95 correlation. Fig. 8 shows the scatter plot comparing the model estimates with the subjective scores.

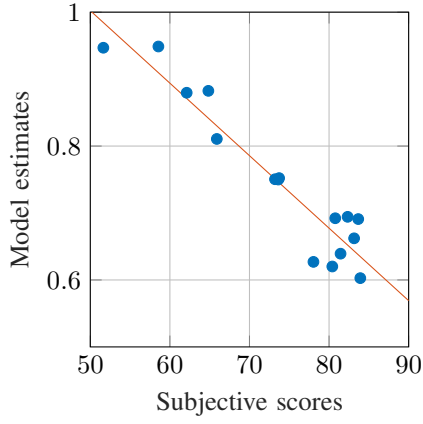


Fig. 8: Scatter plot comparing the subjective scores of the experiment presented in [20] and the estimates of the proposed model. The red line indicates the best-fitting line. The Pearson correlation is -0.95 .

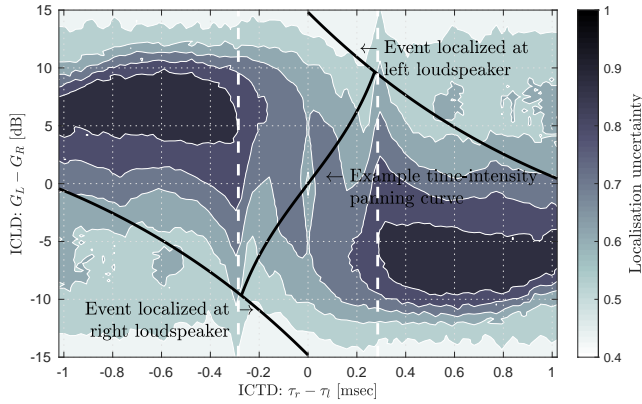


Fig. 9: Contour plot of localization uncertainty as a function of ICLD and ICTD in the center of the sweet-spot. The dashed white lines denote delays that result in the loudspeaker signals arriving at the same time at one of the two ears. Overlaid are the Williams' curves and the time-intensity panning curve associated to the PSR method with $r_m = 0.187$ m.

IV. LOCALIZATION UNCERTAINTY IN STEREOPHONIC REPRODUCTION

A. Localization uncertainty in the center of the sweet-spot

Fig. 9 shows the localization uncertainty produced by the proposed model for a listener in the center of the sweet-spot and for a stereophonic reproduction system with base angle $\phi_0 = 60^\circ$ and $r_l = 2$ m (see Fig. 1). Two areas in the second and fourth quadrants have a significant localization uncertainty. These areas correspond to cases where ICLD and ICTD provide inconsistent information—one loudspeaker is leading in terms of ICLD (i.e. it is louder) while the other is leading in terms of ICTD (i.e. it arrives earlier). This indicates that inconsistent ICTD-ICLD pairs somehow translate to unnatural ITD-ILD cues, which is in agreement with the experimental findings of Leakey in [50]. It may also be observed in Fig. 9 that large ICLD values (outside $\approx \pm 13$ dB) result in a low localization uncertainty for all ICTDs. Here, one loudspeaker

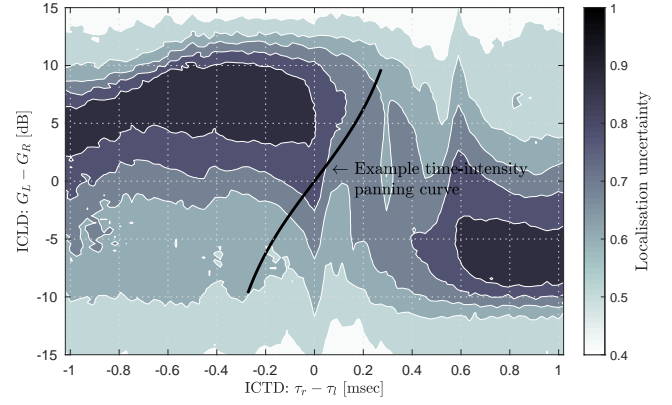


Fig. 10: Contour plot of localization uncertainty as a function of ICLD and ICTD in the off-center position $\mathbf{x} = \{0.1, 0\}$ m (see Fig. 1). Overlaid is the time-intensity panning curve associated to the PSR method with $r_m = 0.187$ m.

signal is masking the other.

Finally, it can be observed that for ICTDs around ± 0.3 ms the localization uncertainty increases even in the first and third quadrants, where ICTDs-ICLDs pairs are consistent. At ICTDs of approximately ± 0.3 ms, the two loudspeaker signals arrive at the same time at one of the two ears (more specifically, at the left ear for $\text{ICTD} \approx +0.3$ ms and at the right ear for $\text{ICTD} \approx -0.3$ ms). Appendix A proves that these ICTDs can be approximated as

$$\tau_o \approx \pm \frac{r_h}{c} \left[\cos \left(\theta_e - \frac{\phi_0}{2} \right) + \frac{\phi_0}{2} + \theta_e - \frac{\pi}{2} \right], \quad (16)$$

where r_h denotes the head radius and θ_e denotes the angle between the forward-looking direction and the ear. For $r_h = 0.09$ m, $\theta_e = 100^\circ$ and $\phi_0 = 60^\circ$, then $\tau_o = \pm 0.27$ ms. If signals of both loudspeakers arrive at the same time at one of the ears, that ear effectively receives one instance of the rendered acoustic event, whereas the other ear receives two instances. A number of psychoacoustic studies investigated effects of presenting three coherent stimuli, two to one ear and the third to the other ear. It was found that the perceived event had “complex spatial structure” including cases where, depending on relative delays between the three stimuli, two distinct acoustic sources could be perceived [4]. The results of the proposed model are in agreement with the findings of these experiments. In fact, simulations not shown here for space reasons, confirm that as the head radius r_h changes, the areas with higher ICTDs in the first and third quadrants move in accordance to (16). If one wishes to avoid these areas, the ICTD values should be restricted to the open interval $\text{ICTD} \in] -\tau_o, \tau_o[$.

In Fig. 9, notice how the PSR panning curve associated to $r_m = 0.187$ m avoids the areas with high localization uncertainty around $\text{ICTD} \approx \pm 0.3$ ms. This is so by construction, as will be discussed later in Section V-A.

B. Localization uncertainty in off-center positions

Figures 10 and 11 show the localization uncertainty for a listener in a position 0.1 m and 0.2 m to the right of the

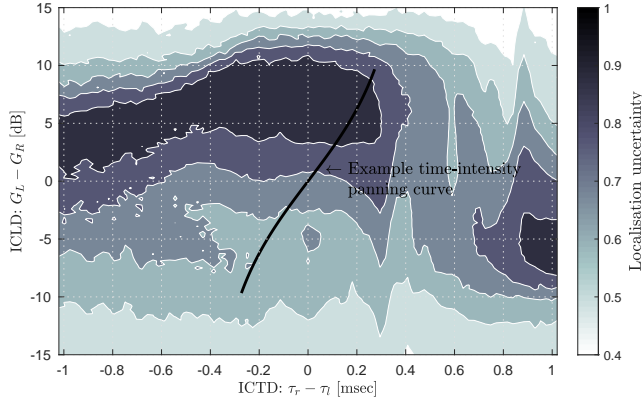


Fig. 11: Contour plot of localization uncertainty as a function of ICLD and ICTD in the off-center position $\mathbf{x} = \{0.2, 0\}$ m (see Fig. 1). Overlaid is the time-intensity panning curve associated to the PSR method with $r_m = 0.187$ m.

sweet-spot, respectively. The listener is still looking ahead, in a direction parallel to the y-axis. It may be observed that both plots are almost identical to the on-center plot of Fig. 9 but shifted horizontally to the right. This implies that the dominant effect is the change in the ICTDs observed by the listener as a consequence of having moved closer to the right loudspeaker. The change in observed ICLDs, on the other hand, appears to have a minor effect. Likewise, the relative change of direction of the loudspeakers also appears to have a minor effect (in the 0.2 m position, the two loudspeakers appear at 25° and -35° with respect to the listener, compared to $\pm 30^\circ$ for the central position).

Notice how intensity panning methods, which are associated to the line $\text{ICTD} = 0$ ms (corresponding to the y-axis), lie in an area with increased localization uncertainty for both off-center positions. This is especially so for positive ICLD values, which are meant to render phantom sources between the midline and the left loudspeaker (i.e. the far loudspeaker in this case). Notice also how the PSR panning curve associated to $r_m = 0.187$ m largely avoids areas with high localization uncertainty in the position 0.1 m off-center.

Finally, notice how the bottom half of the plane has a lower overall localization uncertainty. This is the area of the plot where one renders phantom sources in between the midline and the right loudspeaker (the near loudspeaker).

C. Definition of relative inter-channel time and level differences

In order to aid the interpretation of Figures 10 and 11, it is useful to define two new quantities: the *relative* ICTD and ICLD, i.e. equivalent inter-channel time and level difference as they are observed at a point away from the center of the loudspeaker array. These quantities will be referred to as relative inter-channel time difference (RICTD) and relative inter-channel level difference (RICLD), respectively.

Let the observation point be positioned at (x, y) (see Fig. 1). Appendix B provides a closed-form approximation for the RI-

CLD and RICTD under the assumption of small displacement compared to the loudspeaker distance:

$$\begin{aligned} \text{RICLD} &\approx \text{ICLD} - \frac{x}{r_l} \frac{20 \sin\left(\frac{\phi_0}{2}\right)}{\log_e(10)}, \\ \text{RICTD} &\approx \text{ICTD} - x \frac{2}{c} \sin\left(\frac{\phi_0}{2}\right). \end{aligned} \quad (17)$$

D. Considerations on the effect of RICTD and RICLD in intensity panning

Consider now again the 0.1 m off-center plot in Fig. 10. The point $\text{ICTD} = 0$ ms and $\text{ICLD} = 5$ dB (i.e. the left loudspeaker leads in amplitude) is associated to $\text{RICTD} = -0.29$ ms and $\text{RICLD} = 4.7829$ dB, which have opposite sign and thus provide inconsistent information. The RICLD is now smaller than $\text{ICLD} = 5$ dB because the right loudspeaker is closer to the listener. The change, however, is small (0.22 dB), and the left loudspeaker still leads in amplitude. The RICTD , on the other hand, has changed significantly with respect to ICTD , and the right loudspeaker is now leading in time. To summarise, the left loudspeaker is louder and thus leads in terms of amplitude, but the right loudspeaker is now closer and thus leads in terms of time. Even though the ICTD and ICLD were consistent, the horizontal shift of the observer caused the RICTD and RICLD to become inconsistent, which, in turn, led to a high localization uncertainty.

Negative values of ICLD , on the other hand, are less problematic in terms of localization uncertainty for a listener in this position. For instance, $\text{ICTD} = 0$ ms and $\text{ICLD} = -5$ dB is associated to relative values $\text{RICTD} = -0.29$ ms and $\text{RICLD} = -5.2171$ dB, which have the same sign and provide consistent information.

Similar arguments can be made for a listener moving to the left (i.e. $x < 0$). In this case, however, the plots shift horizontally to the *left* and the critical area of the plot becomes the bottom one. In summary, intensity methods lead to higher localization uncertainty whenever the listener moves to one side but aims to render sound sources in directions closer to the opposite side. Section IV will show that time-intensity methods provide a lower localization uncertainty in positions away from the center of the sweet-spot.

E. Further considerations on RICTD and RICLD

Notice how the RICLD is a function of $\frac{x}{r_l}$, while the RICTD is independent from r_l . This implies that for large loudspeaker arrays, movement of the observation point away from the center of the sweet-spot causes a larger change of RICTD compared to RICLD . This holds also even for living-room-sized arrays. Consider for instance the RICTD that will result in full perceived shift of the phantom source to one loudspeaker, i.e. $\text{RICTD} = 1$ ms. Assuming $\text{ICTD} = 0$ ms, $\text{ICLD} = 0$ dB and $\phi_0 = \pi/3$ (60 degrees), this is already achieved at $x = \frac{0.001c}{2 \sin(\phi_0/2)} = 0.34$ m. In that position, the RICLD , on the other hand, is only 1.5 dB. In other words, a phantom source that appears halfway between loudspeakers for a listener in the center of the sweet-spot, collapses onto one of the loudspeakers when the listener moves to a position

0.34 m on either side. This compares to approximately 0.03 m on either side for binaural cross-talk cancellation using two loudspeakers [51]. It should be noted that the degradation is gradual in both cases, which makes defining quantitatively the sweet-spot size difficult.

Vertical displacement is less significant than horizontal displacement. This can be inferred by the fact that the first-order approximation (17) does not depend on y (it can be shown that y appears starting from the second-order term). For this reason, the simulations in the remainder of the paper will focus on listener displacement along the x axis ($y = 0$).

V. TIME-INTENSITY PANNING/RECORDING METHODS

This section will show how small ICTDs allow to render consistent RICLD-RICTD values (and thus a lower localization uncertainty) in a slightly larger area around the center of the sweet-spot. Towards this end it is convenient to choose a certain parametrization for the ICTD and ICLD. Let this parametrization be defined by equations (1) and (4), reported here with the explicit dependence on r_m :

$$\text{ICTD}(\theta_s, r_m) = 2 \frac{r_m}{c} \sin\left(\frac{\phi_0}{2}\right) \sin \theta_s, \quad (18)$$

$$\text{ICLD}(\theta_s, r_m) = 20 \log_{10} \frac{\sin\left(\frac{\phi_0}{2} + \beta(r_m) + \theta_s\right)}{\sin\left(\frac{\phi_0}{2} + \beta(r_m) - \theta_s\right)}. \quad (19)$$

While this is not the only possible parametrization, this is a convenient choice since it allows to extend the conclusions made in the remainder of this section beyond panning, and into recording with actual microphones.

Notice that instead of the array radius as a parameter, one could have used the inter-microphone distance. This is closer to how stereophonic recording is usually described in the audio engineering literature. The advantage of the parametrization in terms of array radius is that it makes the extension to multi-channel systems trivial, as will be discussed at the end of this section. One can easily switch between parametrizations by observing that the inter-microphone distance is $2r_m \sin(\phi_0/2)$.

The result of this procedure is a family of panning curves parametrized by the value of the microphone array radius r_m . In the extreme case $r_m = 0$, one obtains an intensity-only method ($\text{ICTD}(\theta_s) = 0 \forall \theta_s$). As the value of r_m increases, the ICTDs increase while the ICLDs dictated by (19) decrease, thus achieving stereophonic rendering with a different time/intensity trading ratio.

A. Effect of time/intensity trading on localization uncertainty

Fig. 12 shows the localization uncertainty as a function of array radius r_m and plane wave angle θ_s for three different observation positions. A number of observations can be made.

- As the distance from the center of the sweet spot increases, so does the maximum localization uncertainty.
- In the center position (Fig. 12a), the localization uncertainty is lowest for $r_m = 0$ (i.e. intensity methods) and two “sidebands” appear in the plot beyond $r_m = 0.2$ m. These sidebands correspond to the vertical stripes observed in

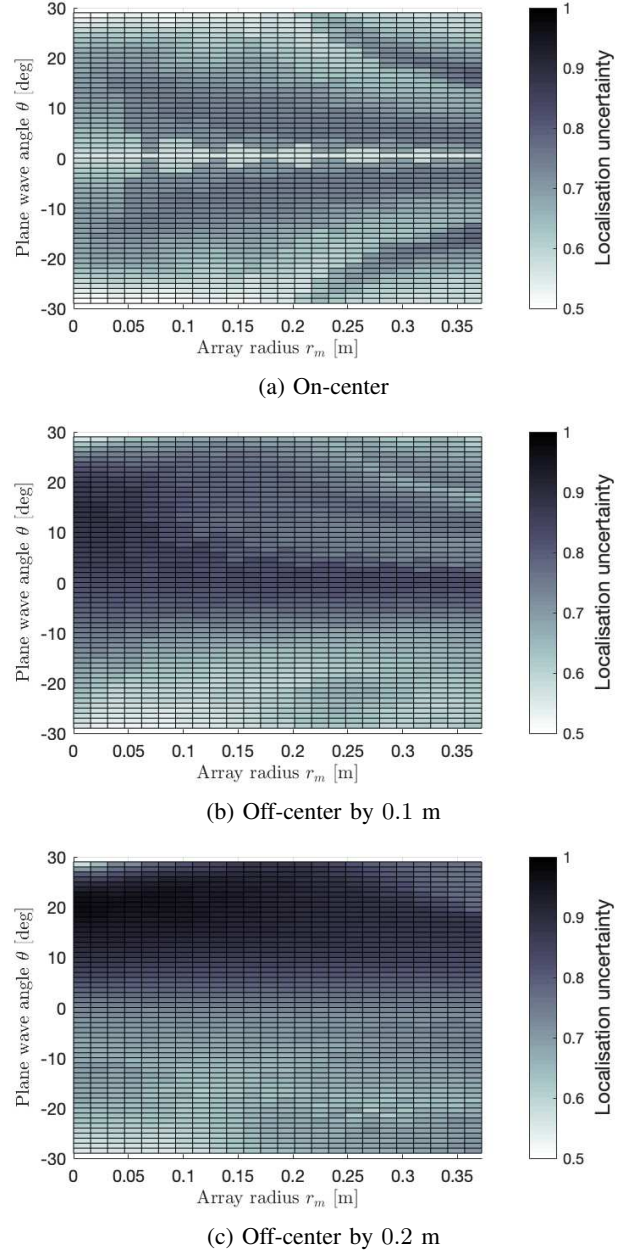


Fig. 12: Localization uncertainty as a function of microphone array radius, r_m , and plane wave angle, θ_s , in (a) the center position, (b) in a position 0.1 m off-center to the right, i.e. $(x, y) = (0.1, 0)$ m, and (c) in a position 0.2 m off-center to the right, i.e. $(x, y) = (0.20, 0)$ m. The colorbar is the same for all three figures so that a relative comparison is possible.

Fig. 9 at $\pm\tau_0$.

- At $x = 0.1$ m (Fig. 12b), the localization uncertainty is highest for array radius $r_m = 0$ m, i.e. intensity methods. It remains high in plane wave directions around the midline, while it reduces for other directions, especially around the $\theta_s \in [10^\circ, 20^\circ]$ range. This can be observed also in Fig. 10, which shows the panning curve associated to $r_m = 0.187$ m. Here, the panning curves avoids the areas with higher localization uncertainty coming in from the left.
- At $x = 0.2$ m (Fig. 12c), the localization uncertainty tends to

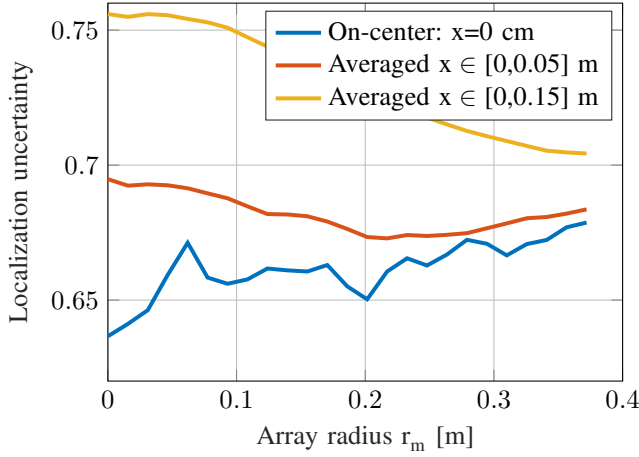


Fig. 13: Localization uncertainty as a function of array radius r_m . Results are averaged across angles between the midline and the left loudspeaker.

reduce for higher r_m and in a more uniform manner across angles θ_s .

Fig. 13 shows the localization uncertainty averaged across directions θ_s . Here the results are averaged across angles between the midline and the left loudspeaker, which are more difficult to render when the listener moves to the right of the center. The curve associated to the center position shows that, in that position, the radius with the lowest uncertainty is the one $r_m = 0$ m, as expected. Around $r_m = 0.2$ m the uncertainty has a dip before increasing further, which is due to the sidebands of Fig. 9.

In typical use cases, one would like to minimize the uncertainty as it is observed in a whole region around the center of the sweet spot, instead of specific positions. Fig. 13 shows the localization uncertainty averaged for listener displacements between $x = 0$ m and $x = 0.05$ m. The average uncertainty is still low for $r_m = 0$ m, but the absolute minimum is achieved at $r_m = 0.2$ m. Fig. 13 also shows the localization uncertainty averaged for displacements between $x = 0$ m and $x = 0.15$ m. In this case, the average uncertainty increases significantly at small radii, and the absolute minimum moved to $r_m \approx 0.35$ m.

In summary, the results suggest that smaller radii (intensity methods) are preferable for positions close to the center, while larger radii result in lower localization uncertainty at larger distances. There is thus a trade off between lower localization uncertainty in the center of the sweet spot and away from the center.

Unless one is actively tracking the listener, in most application of interest it is difficult to predict how far the listener will move away from the center of the sweet spot. A possible compromise is to use the largest array radius that results in the extreme ICTD to be no larger than τ_o , and thus avoid the areas with higher localization uncertainty in the first and third quadrant shown in Fig. 9. One can find this array radius by equating ICTD_{\max} with τ_o , and isolating r_m :

$$r_m = r_h \frac{\cos\left(\theta_e - \frac{\phi_0}{2}\right) + \frac{\phi_0}{2} + \theta_e - \frac{\pi}{2}}{2 \sin^2\left(\frac{\phi_0}{2}\right)}. \quad (20)$$

For instance, the array radius for $\theta_e = 100^\circ$ and $r_h = 0.09$ m, is $r_m = 0.187$ m, which is the radius used for the panning curve shown in figures 9, 10 and 11.

B. Extension to multichannel

The stereophonic setup considered thus far can be seen as a subset of a multichannel circular array. In [20], it was shown that for a given direction, having only the two closest loudspeakers as active yields a lower spatial fluctuation of the active intensity vector field and thus a larger sweet spot. This turns the overall multichannel design problem into a number of stereophonic problems.

Consider the case of N microphones distributed uniformly around the circle with $\phi_0 = 2\pi/N$. Each of these microphones is connected to a loudspeaker in the same angular configuration, without mixing. Johnston and Lam proposed in [21] a microphone array with $N = 5$, resulting in a base angle of $\phi_0 = 2\pi/5 = 72^\circ$, and radius 0.155 m. This radius is very close to the value obtained from equation (20): $r_m = 0.162$ m (notice that the difference with $r_m = 0.187$ m used elsewhere in this paper is due to the different base angles). Johnston and Lam stated that $r_m = 0.155$ m would conserve ITD cues that the listener would have experienced in the recording space, but without providing a rigorous explanation (it could indeed be argued, as Bernfeld did in [45], that correct ITD cues can also be achieved by using ICLDs alone). This paper shows that Johnston and Lam's choice of array radius is the one that leads to a good compromise between low localization uncertainty in central and non-central listener positions. The same choice was made in [20], where the directional accuracy was also improved significantly.

VI. SUMMARY AND CONCLUSIONS

This paper focused on the effect of inter-channel time and level differences on perceived localization uncertainty. A computational model was proposed, based on calculating a distance functional between the observed ILD-ITD values and the ones associated to free-field sound sources. The distance functional was chosen as the 0.3-norm which is capable of modelling the splitting of auditory events observed experimentally in case of contradicting ILD-ITD cues. The model predictions had a high correlation with results of formal listening experiments. The model can also be used to predict the perceived localization angle, but this is left to future research.

The model was then used to predict the localization uncertainty under stereophonic reproduction. It was found that a high localization uncertainty was associated with (a) contradicting ICTD-ICLD pairs and (b) ICTDs resulting in the loudspeaker signals overlapping in time at either ear. Closed form approximations of the ICTDs and ICLDs relative to the listener (denoted as RICTD and RICLD) were presented. It was observed that when a listener moves away from the center of the sweet-spot, the RICLD remains largely unchanged, while the RICTD changes even for small displacements. In off-center positions, then, one can obtain contradicting RICLD-RICTD pairs even if the original ICLD-ICTD pairs were not. It was then explained that non-zero ICTDs (i.e. time-intensity

methods) will delay the onset of contradicting RICLD and RICTD. More significant use of ICTDs results in a higher uncertainty in the center of the sweet-spot, but a relatively lower one in off-center positions.

This result may help reconcile the long-standing debate between the academia, which tends to adopt intensity methods (e.g. VBAP, Ambisonics, SDM), and the audio recording industry, which supports both intensity and time-intensity methods (e.g. Decca tree [5], [7]).

In this paper it was not possible to analyze widely spaced microphone arrays such as the ones criticized by Lipshitz [11] or time panning as criticized by Lee and Rumsey [10], since they exceed the 1 ms ICTD limit beyond which one has to also model the law of the first front. This paper is therefore not in contradiction with the findings in [11] and [10], as the conclusions made here are limited to coincident and near-coincident microphone arrays. The computational model could be modified to account for the law of the first front, e.g. by means of inhibitions mechanisms [33], thus allowing analysis of widely spaced microphone arrays.

Throughout this paper, it was implicitly assumed that a low localization uncertainty is desirable. This is motivated by the fact that an actual plane wave is well localized spatially, and that to render it accurately it needs to have a low localization uncertainty. This may not be necessarily the case e.g. in an artistic context, where one may prefer to render sound sources as difficult to localize. The results in this paper are useful in this context too as they can also be read with an implicit preference for high uncertainty.

APPENDIX A

This appendix provides a closed-form approximation of the ICTD that results in the two loudspeaker signals to arrive at the same time at the left ear. Let the head radius be denoted by r_h and the angle between the forward-looking direction and the ear be denoted by θ_e . Let $\theta_0 = \cos^{-1}\left(\frac{r_h}{r_l}\right)$ be the angle of tangential incidence on the spherical head. Assuming that $\left|\frac{r_h}{r_l}\right| \ll 1$, i.e. the head radius is much smaller than the loudspeaker distance, then $\theta_0 \approx \frac{\pi}{2}$.

The angle between the left loudspeaker and the left ear is $\theta_{LL} = \theta_e - \frac{\phi_0}{2}$ and under most conditions, $\theta_{LL} < \theta_0$. The distance between the left loudspeaker and the left ear is then:

$$d_{LL} = \sqrt{r_l^2 + r_h^2 - 2rr_h \cos(\theta_{LL})} \quad (21)$$

$$= r_l \sqrt{1 + \frac{r_h^2}{r_l^2} - 2\frac{r_h}{r_l} \cos\left(\theta_e - \frac{\phi_0}{2}\right)} \quad (22)$$

$$\approx r_l - r_h \cos\left(\theta_e - \frac{\phi_0}{2}\right), \quad (23)$$

where in the last step, the quadratic term $\frac{r_h^2}{r_l^2}$ is ignored and the square root is approximated using the first-order Taylor series approximation.

The angle between the right loudspeaker and the left ear is $\theta_{RL} = \frac{\phi_0}{2} + \theta_e$ and under most conditions, $\theta_{RL} > \theta_0$. The distance between the right loudspeaker and the left ear, then, is given by the summation of the distance between the

loudspeaker and the point of tangential incidence, and the remaining angular sector:

$$d_{RL} = \sqrt{r_l^2 + r_h^2} + r_h(\theta_{RL} - \theta_0). \quad (24)$$

For small $\frac{r_h}{r_l}$, the quadratic term $\left(\frac{r_h}{r_l}\right)^2$ can be ignored:

$$d_{RL} \approx r_l + r_h \left(\frac{\phi_0}{2} + \theta_e - \frac{\pi}{2} \right). \quad (25)$$

The delay applied to the left loudspeaker, τ_o , that makes the two loudspeaker signals arrive at the same time at the left ear satisfies the equation

$$\frac{d_{LL}}{c} + \tau_o = \frac{d_{RL}}{c}. \quad (26)$$

Replacing equations (23) and (25), and solving for τ_o yields

$$\tau_o \approx \frac{r_h}{c} \left[\cos\left(\theta_e - \frac{\phi_0}{2}\right) + \frac{\phi_0}{2} + \theta_e - \frac{\pi}{2} \right]. \quad (27)$$

Due to the symmetry of the problem, if one applies the same delay τ_o multiplied by -1 , then the loudspeaker signals will arrive at the same time at the right ear.

APPENDIX B

This appendix provides a closed-form approximation of the RICTD and RICLD. Towards this end, approximations of the relative distance between an observation point (x, y) and the two loudspeakers at a distance r_l from the center of the sweet-spot $(0, 0)$ are sought first. It will be assumed that $\left|\frac{x}{r_l}\right| \ll 1$ and $\left|\frac{y}{r_l}\right| \ll 1$. The distance between the observation point (x, y) and the right loudspeaker can be approximated as

$$d_R^2 = \left(r_l \sin\left(\frac{\phi_0}{2}\right) - x \right)^2 + \left(r_l \cos\left(\frac{\phi_0}{2}\right) - y \right)^2 \quad (28)$$

$$\approx r_l^2 \left[1 - 2\frac{x}{r_l} \sin\left(\frac{\phi_0}{2}\right) - 2\frac{y}{r_l} \cos\left(\frac{\phi_0}{2}\right) \right], \quad (29)$$

where in the second step it is assumed that $\left(\frac{x}{r_l}\right)^2 \approx 0$, and $\left(\frac{y}{r_l}\right)^2 \approx 0$. It is useful to define $a = 2\frac{x}{r_l} \sin\left(\frac{\phi_0}{2}\right)$ and $b = 2\frac{y}{r_l} \cos\left(\frac{\phi_0}{2}\right)$, so that d_R can be rewritten as $d_R \approx r_l \sqrt{1 - (a + b)}$. The first-order Taylor series approximation of the square root yields:

$$d_R \approx r_l \left(1 - \frac{a + b}{2} \right) \quad (30)$$

Using similar steps, d_L can be approximated by $d_L \approx r_l \left(1 + \frac{a - b}{2} \right)$. The time delay between the two loudspeakers observed in (x, y) can now be approximated as

$$\frac{d_R - d_L}{c} \approx -\frac{r_l a}{c} = -x \frac{2}{c} \sin\left(\frac{\phi_0}{2}\right). \quad (31)$$

The relative level observed in (x, y) for the two point-like loudspeakers can now be approximated as

$$20 \log_{10} \left(\frac{\frac{1}{d_L}}{\frac{1}{d_R}} \right) \approx 20 \log_{10} \frac{1 - \frac{x}{2r_l} \sin\left(\frac{\phi_0}{2}\right) - \frac{y}{2r_l} \cos\left(\frac{\phi_0}{2}\right)}{1 + \frac{x}{2r_l} \sin\left(\frac{\phi_0}{2}\right) - \frac{y}{2r_l} \cos\left(\frac{\phi_0}{2}\right)}, \quad (32)$$

and, using a first-order Taylor series approximation:

$$20 \log_{10} \left(\frac{\frac{1}{d_L}}{\frac{1}{d_R}} \right) \approx -\frac{x}{r_l} \frac{20}{\log_e(10)} \sin \left(\frac{\phi_0}{2} \right), \quad (33)$$

Using (31) and (33), one obtains $\text{RICLD} \approx \text{ICLD} - \frac{x}{r_l}$ and $\text{RICTD} \approx \text{ICTD} - x \frac{2}{c} \sin \left(\frac{\phi_0}{2} \right)$.

REFERENCES

- [1] E. De Sena and Z. Cvetković, "A computational model for the estimation of localisation uncertainty," in *Proc. IEEE Int. Conf. on Acoust. Speech and Signal Process. (ICASSP-13)*, Vancouver, Canada, May 2013, pp. 388–392.
- [2] E. De Sena, "Analysis, design and implementation of multichannel audio systems," Ph.D. dissertation, King's College London, 2013.
- [3] H. Hacıhabiboğlu, E. De Sena, Z. Cvetković, J. Johnston, and J. Smith, "Perceptual spatial audio recording, simulation, and rendering: An overview of spatial-audio techniques based on psychoacoustics," *IEEE Signal Processing Magazine*, vol. 34, no. 3, pp. 36–54, 2017.
- [4] J. Blauert, *Spatial Hearing: The Psychophysics of Human Sound Localization*. MIT Press, 1997.
- [5] F. Rumsey, *Spatial audio*. Focal Press, 2001.
- [6] V. Pulkki, "Virtual sound source positioning using vector-base amplitude panning," *J. Audio Eng. Soc.*, vol. 45, no. 6, pp. 456–466, Jun. 1997.
- [7] J. Eargle, *The microphone book*. Focal Press, 2004.
- [8] J. Daniel, J. Rault, and J. Polack, "Ambisonics encoding of other audio formats for multiple listening conditions," presented at the 105th Audio Eng. Soc. Conv., Preprint #4795, San Francisco, CA, USA, Sep. 1998.
- [9] S. Tervo, J. Pätynen, A. Kuusinen, and T. Lokki, "Spatial decomposition method for room impulse responses," *J. Audio Eng. Soc.*, vol. 61, no. 1/2, pp. 17–28, 2013.
- [10] H. Lee and F. Rumsey, "Level and time panning of phantom images for musical sources," *J. Audio Eng. Soc.*, vol. 61, no. 12, pp. 978–988, 2013.
- [11] S. P. Lipshitz, "Stereo microphone techniques: Are the purists wrong?" *J. Audio Eng. Soc.*, vol. 34, no. 9, pp. 716–744, May 1986.
- [12] F. Rumsey and T. McCormick, *Sound and recording: applications and theory*. Focal Press, 2014.
- [13] M. Plewa and P. Kleczkowski, "Choosing and configuring a stereo microphone technique based on localisation curves," *Archives of Acoustics*, vol. 36, no. 2, pp. 347–363, 2011.
- [14] H. Wittek and G. Theile, "Development and application of a stereophonic multichannel recording technique for 3d audio and vr," in *presented at the 143rd Audio Eng. Soc. Conv.* Audio Engineering Society, 2017.
- [15] L. Riitano, M. Victoria, and J. Enrique, "Comparison between different microphone arrays for 3d-audio," in *presented at the 144th Audio Eng. Soc. Conv.* Audio Engineering Society, 2018.
- [16] M. Williams, *Microphone Array Analysis for Stereo and Multichannel Sound Recording*. Editrice Il Rostro, 2004, vol. 1.
- [17] H. Lee, "Capturing 360 audio using an equal segment microphone array (esma)," *J. Audio Eng. Soc.*, vol. 67, no. 1/2, pp. 13–26, 2019.
- [18] C. Millns and H. Lee, "An investigation into spatial attributes of 360° microphone techniques for virtual reality," in *presented at the 144th Audio Eng. Soc. Conv.*, 2018.
- [19] H. Lee, D. Johnson, and M. Mironovs, "An interactive and intelligent tool for microphone array design," in *presented at the 143rd Audio Eng. Soc. Conv.*, 2017.
- [20] E. De Sena, H. Hacıhabiboğlu, and Z. Cvetković, "Analysis and design of multichannel systems for perceptual sound field reconstruction," *IEEE Trans. on Audio, Speech and Language Process.*, vol. 21, no. 8, pp. 1653–1665, Aug. 2013.
- [21] J. D. Johnston and Y. H. Lam, "Perceptual soundfield reconstruction," presented at the 109th Audio Eng. Soc. Conv., Preprint #2399, Los Angeles, CA, USA, Sep. 2000.
- [22] H. Hacıhabiboğlu and Z. Cvetković, "Panoramic recording and reproduction of multichannel audio using a circular microphone array," in *Proc. 2009 IEEE Workshop on Appl. of Signal Process. to Audio and Acoust. (WASPAA'09)*, Oct. 2009, pp. 117–120.
- [23] G. W. Elko, "Differential microphone arrays," in *Audio signal processing for next-generation multimedia communication systems*, Y. Huang and J. Benesty, Eds. Kluwer Academic Publishers, 2004.
- [24] E. De Sena, H. Hacıhabiboğlu, and Z. Cvetković, "On the design and implementation of higher order differential microphones," *IEEE Trans. on Audio, Speech and Language Process.*, vol. 20, no. 1, pp. 162–174, Jan. 2012.
- [25] S. Bech and N. Zacharov, *Perceptual Audio Evaluation: Theory, Method and Application*. John Wiley & Sons, 2006.
- [26] R. Y. Litovsky, H. S. Colburn, W. A. Yost, and S. J. Guzman, "The precedence effect," *J. Acoust. Soc. Am.*, vol. 106, no. 4, pp. 1633–1654, Oct. 1999.
- [27] M. B. Gardner, "Historical background of the Haas and/or precedence effect," *J. Acoust. Soc. Am.*, vol. 43, no. 6, pp. 1243–1248, 1968.
- [28] M. Williams and G. Le Du, "Microphone array analysis for multichannel sound recording," presented at the 107th Audio Eng. Soc. Conv., Preprint #4997, New York, USA, Sep. 1999.
- [29] N. V. Franssen, *Stereophony*. Philips Research Laboratories, 1964.
- [30] L. Simon and R. Mason, "Time and level localization curves for a regularly-spaced octagon loudspeaker array," presented at the 128th Audio Eng. Soc. Conv., Preprint #8079, London, UK, May 2010.
- [31] H. Hacıhabiboğlu, E. De Sena, and Z. Cvetković, "Design of a circular microphone array for panoramic audio recording and reproduction: Microphone directivity," presented at the 128th Audio Eng. Soc. Conv., Preprint #8063, London, UK, May 2010.
- [32] L. A. Jeffress, "A place theory of sound localization," *J. of Comparative and Physiological Psychology*, vol. 41, no. 1, p. 35, February 1948.
- [33] W. Lindemann, "Extension of a binaural cross-correlation model by contralateral inhibition. i. simulation of lateralization for stationary signals," *J. Acoust. Soc. Am.*, vol. 80, pp. 1608–1622, Jul. 1986.
- [34] W. Gaik, "Combined evaluation of interaural time and intensity differences: Psychoacoustic results and computer modeling," *J. Acoust. Soc. Am.*, vol. 94, no. 1, pp. 98–110, Jul. 1993.
- [35] V. Pulkki and T. Hirvonen, "Localization of virtual sources in multichannel audio reproduction," *IEEE Trans. on Audio, Speech and Language Process.*, vol. 13, no. 1, pp. 105–119, Jan. 2005.
- [36] C. Fallér and J. Merimaa, "Source localization in complex listening situations: Selection of binaural cues based on interaural coherence," *J. Acoust. Soc. Am.*, vol. 116, p. 3075, Jul. 2004.
- [37] R. O. Duda and W. L. Martens, "Range dependence of the response of a spherical head model," *J. Acoust. Soc. Am.*, vol. 104, pp. 3048–3058, Nov. 1998.
- [38] M. Slaney, "An efficient implementation of the Patterson-Holdsworth auditory filter bank," *Apple, Perception Group, Tech. Rep.*, 1993.
- [39] B. R. Glasberg and B. C. J. Moore, "Derivation of auditory filter shapes from notched-noise data," *Hearing research*, vol. 47, no. 1, pp. 103–138, Aug. 1990.
- [40] A. N. Kolmogorov and S. V. Fomin, *Elements of the theory of functions and functional analysis*. Dover Publications, 1999.
- [41] I. R. Goodman and S. Kotz, "Multivariate θ -generalized normal distributions," *J. of Multivariate Analysis*, vol. 3, no. 2, pp. 204–219, 1973.
- [42] J. D. Johnston, "Transform coding of audio signals using perceptual noise criteria," *IEEE J. on Selected Areas in Comm.*, vol. 6, no. 2, pp. 314–323, 1988.
- [43] S. M. Kay, *Fundamentals of Statistical Signal Processing: Estimation Theory*. Pearson Education, 1993.
- [44] Various, *Recomm. BS.1534-1, Method for the subjective assessment of intermediate quality level of coding systems*. ITU-R, 2003.
- [45] B. Bernfeld, "Attempts for better understanding of the directional stereophonic listening mechanism," presented at the 44th Audio Eng. Soc. Conv., Preprint #C-4, Rotterdam, the Netherlands, Mar. 1973.
- [46] J. Daniel, "Spatial sound encoding including near field effect: Introducing distance coding filters and a viable, new ambisonic format," in *Proc. 23rd Audio Eng. Soc. Int. Conf.*, Copenhagen, Denmark, May 2003.
- [47] M. Poletti, "A unified theory of horizontal holographic sound systems," *J. Audio Eng. Soc.*, vol. 48, no. 12, pp. 1155–1182, Dec. 2000.
- [48] J. Daniel, "Représentation de champs acoustiques, application à la transmission et à la reproduction de scènes sonores complexes dans un contexte multimédia," Ph.D. dissertation, Univ. of Paris VI, France, July 2000.
- [49] B. Gardner and K. Martin, "HRTF measurements of a kemar dummy-head microphone," MIT Media Lab Perceptual Computing - Technical Report 280, Tech. Rep., May 1994.
- [50] D. M. Leakey, "Some measurements on the effects of interchannel intensity and time differences in two channel sound systems," *J. Acoust. Soc. Am.*, vol. 31, no. 7, pp. 977–986, 1959.
- [51] J. Rose, P. Nelson, B. Rafaely, and T. Takeuchi, "Sweet spot size of virtual acoustic imaging systems at asymmetric listener locations," *J. Acoust. Soc. Amer.*, vol. 112, no. 5, pp. 1992–2002, 2002.